Reports

Elimination of Current Dissipation in High Transition Temperature Superconductors

J. Z. SUN, B. LAIRSON, C. B. EOM, J. BRAVMAN, T. H. GEBALLE

The relaxation of the shielding current–induced magnetic moment in $YBa_2Cu_3O_7$ thin films, which were grown in situ, is studied as a function of temperature. Although typical relaxations cause a large amount of decay in the magnetic shielding current (on the order of 10 to 20 percent for the first 1000 seconds), it is shown that this is not necessarily a serious problem for applications such as magnets operating in persistent-current modes. This is because the decay of the magnetic shielding current depends sensitively on how far away the operating current density is from the critical current density J_c. By using a quenching process the shielding current is reduced slightly below J_c and the relaxation is dramatically reduced. A general relation between the relaxation rate at J_c and the reduction of the relaxation rate upon lowering of the operating current is obtained and is shown to be consistent with experimental data.

SIGNIFICANT RELAXATION OF THE magnetic shielding current has been widely seen on $YBa_2Cu_3O_7$ (YBCO) bulk materials (*1–6*) and even in high critical current density thin films (*7, 8*). This causes some concerns regarding the applicability of the high transition temperature (T_c) superconducting oxide materials to systems requiring a persistent supercurrent—systems such as low noise superconducting magnets. However, because all these relaxation experiments were performed in the condition such that the current density inside the specimen was very close to the critical density J_c, they only revealed sample quality in the worst limit (performance at full J_c). In this report we present our studies on the relaxation of the magnetic shielding current not only at J_c but also in the region where the actual shielding current is slightly below J_c. This reduces the relaxation rate dramatically due to the reduction of the dissipation level.

Test samples of YBCO were grown epitaxially on (100) MgO substrates using in situ sputter deposition from a stoichiometric YBCO target with the off-axis geometry (*9*). These films typically have a size of 0.6 cm by 0.6 cm by 4000 Å with a T_c of 86 K measured as zero resistance. Structural studies confirmed that these films are highly textured with the *c*-axis of the YBCO cell perpendicular to the surface of the film. The critical current density J_c was obtained through the Bean critical state model (*10*) by measuring the magnetic hysteresis on a modified Princeton Applied Research model 155 vibration sample magnetometer with fields up to 18 kG applied perpendicular to the surface of the film. The validity of the critical state model has been examined carefully and agreements between transport and magnetically measured J_c was confirmed in the low current density limit (*11*). The J_c at 6 kG thus obtained is shown in Fig. 1 as a function of temperature.

The decay of the magnetic shielding current was studied by first ramping the magnetic field to a certain value to saturate the sample into its critical state and then, immediately after, recording the magnetic moment generated by the shielding current as a function of time. A typical set of such data is shown in Fig. 2 which was taken at 6 kG. As can be seen, the decay rate is roughly logarithmic (*12*) which can be rather well described by the relation

$$M(t) \approx M(0)\left[1 - \frac{1}{n-1}\ln\left(\frac{t}{\tau_1} + 1\right)\right] \quad (1)$$

with $M(0)$ the initial moment and n the exponent reflecting the rate of relaxation. We have shown elsewhere that Eq. 1 follows from the power law–like current-voltage (*J-E*) characteristic which describes the behavior of our samples (*13*). If we assume such a current-voltage characteristic

$$E = \alpha J^n \quad (2)$$

then the time scale τ_1 is determined by (*13*)

$$\tau_1 \approx \frac{\pi l a^3 \Lambda}{3 c M^{n-1}(0)\,\alpha\,(n-1)} \quad (3)$$

with l the sample thickness, a the sample radius (assuming the sample is a round disk), c the speed of light, and $\Lambda \approx 4\pi a^2/c^2$. $M(0)$ is the initial moment that relates to the critical current density through the Bean formula

$$J_c = \frac{3c}{\pi l a^3} M(0) \quad (4)$$

which also relates $J(t)$ to $M(t)$ as long as the current distribution inside the sample is uniform.

Because the sample is in its critical state, the shielding current is pushed all the way up to the critical current density everywhere. To see how much effect a reduction of the shielding current will have upon the relaxation process, a shielding current less than J_c has to be set up. This is done by first driving the sample into its critical state at a certain temperature T_1, and then after a well-defined period of time t_1, suddenly cooling the sample to another temperature $T_2 < T_1$. The decrease of temperature causes an increase in the critical current density, as can be obviously seen from Fig. 1. However, the shielding current is set up before the increase of J_c and is therefore trapped inside the sample with its value below the now increased J_c. This operation results in great reduction of the relaxation rate. Figure 3 demonstrates the result by

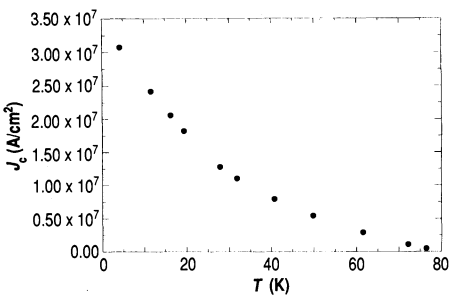

Fig. 1. The typical temperature dependence of the critical current density measured at 6 kG.

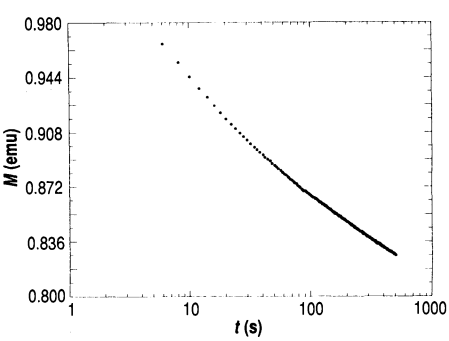

Fig. 2. The decay of magnetic shielding current at 19 K, 6 kG. It is roughly logarithmic in time.

J. Z. Sun and T. H. Geballe, Department of Applied Physics, Stanford University, Stanford, CA 94305.
B. Lairson, C. B. Eom, J. Bravman, Department of Materials Science and Engineering, Stanford University, Stanford, CA 94305.

comparing two decay curves with one taken at 19.2 K all the way out to 500 s and the second quenched to 17.1 K at 24 s after the shielding current was set up at 19.2 K. The temperature variation is completed in about 5 s and the variation was made without undershooting the temperature. As can be seen from the plot, the relaxation rate dM/dt at the point of t_1 is reduced by about a factor of 10. From Fig. 1 it is estimated that such a decrease of temperature increases J_c by only 7.5%, yet its effect on the relaxation is already very significant.

To see how this can be we return to Eq. 1. It can be shown (*12*) that Eq. 1 is the linearized solution of the simplified relaxation equation

$$\Lambda \frac{dJ}{dt} \approx -E = -\alpha J^n \quad (5)$$

with the initial condition of

$$J(t = 0) = J_c \quad (6)$$

It is obvious that what the quench experiment does is simply change the prefactor α in Eq. 5 and the initial condition Eq. 6 at time t_1 (here we assume that the exponent is not a sensitive function of temperature. This is true for YBCO in the temperature region of concern). At t_1, Eq. 5 is changed to

$$\Lambda \frac{dJ}{dt} \approx -\alpha' J^n = -\alpha\eta^n J^n \ (t \geq t_1) \quad (7)$$

with η defined as the operation level which is the ratio between the real shielding current density J (which is close to the J_c before quench) and the critical current density after quench, J_{cQ}:

$$\eta \equiv \frac{J}{J_{cQ}} \approx \frac{J_c}{J_{cQ}} \quad (8)$$

with the initial condition Eq. 6 changed to

$$J(t = t_1) \approx J(0)\left[1 - \frac{1}{n-1}\ln\left(\frac{t_1}{\tau_1} + 1\right)\right] \quad (9)$$

This analysis is limited to situations with $1 - \eta << 1$ since a rather uniform current distribution within the sample is required for the validity of Eq. 5 (*13*). Assuming this, it is easy to see that this change yields a result that is nothing more than Eq. 1 with a shift of origin in time and a modification on the time denominator τ_1:

$$M(t) \approx M(t_1) \times \left[1 - \frac{1}{n-1}\ln\left(\frac{t}{\tau_2} + 1\right)\right] (t \geq t_1) \quad (10)$$

with

$$\tau_2 = \frac{1}{\eta^n\left[1 - \frac{1}{n-1}\ln\left(\frac{t_1}{\tau_1} + 1\right)\right]^{n-1}}\tau_1 \quad (11)$$

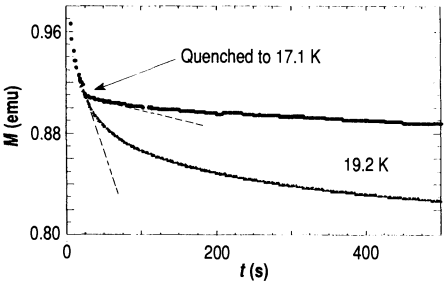

Fig. 3. Bottom curve: isothermal relaxation of the magnetic shielding current at 19.2 K having a relaxation rate (shown by the dashed line) of -1.3×10^{-3} emu/s at $t_1 = 24$ s; top curve: relaxation started at 19.2 K and then quenched rapidly down to 17.1 K at $t_1 = 24$ s. The relaxation rate at t_1 (shown by the dashed line) is reduced now to -1.3×10^{-4} emu/s—reduction by a factor of 10. Both measurements were done with the sample saturated into its critical state at 6 kG.

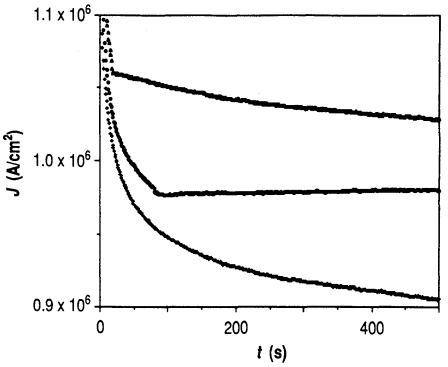

Fig. 4. Decays of the magnetic shielding current with different quench history. Bottom curve: isothermal relaxation at 78.0 K; middle curve: quenched down to 77.5 K at $t_1 \approx 80$ s where $J = 0.98 \times 10^6$ A/cm^2; top curve: quenched down to 77.5 K at $t_1 \approx 20$ s where $J = 1.05 \times 10^6$ A/cm^2.

To compare the relaxation rate before and after quenching we define

$$R_- = \left.\frac{dM}{dt}\right|_{t=t^-_1} \quad (12)$$

to be the slope before quenching at t_1 and

$$R_+ = \left.\frac{dM}{dt}\right|_{t=t^+_1} \quad (13)$$

to be the slope after quenching at t_1. It immediately follows that the ratio of reduction of the relaxation rate

$$\frac{R_-}{R_+} \approx \frac{\tau_2}{t_1} = \frac{\tau_1}{t_1} \times \frac{1}{\left[1 - \frac{1}{n-1}\ln\left(\frac{t_1}{\tau_1} + 1\right)\right]^{n-1}}\left(\frac{1}{\eta^n}\right) \quad (14)$$

Since R_-/R_+ has to equal to one when $\eta = 1$ (that is, the case of no quench), it is obvious that

$$\frac{R_-}{R_+} \approx \left(\frac{1}{\eta}\right)^n \quad (15)$$

From our time dependence data we obtain $n = 38$, $\eta \approx 0.925$ for the quench shown in Fig. 3. With these parameters Eq. 20 predicts that the reduction of the relaxation rate will be of the order 20. This is compared with the actual experimental value of around 10. Considering the fact that it is difficult to determine the accurate value of η (since the final result depends so sensitively on it) and that the quench is not instantaneous, the agreement is reasonable.

Further experiments were carried out at liquid nitrogen temperature. The sample was cycled into the critical state from 400 G to 40 G of applied field at a temperature $T_1 = 78.0$ K, allowed to decay for a time t_1, and then quenched to a lower temperature $T_2 = 77.5$ K. Quenching in this temperature region was accomplished by depressurizing a small nitrogen bath from approximately 1 psi. Figure 4 illustrates this process for $t_1 > 500$ s (no quench), $t_1 = 20$ s, and $t_1 = 80$ s, respectively. Variations in the decay rate before quenching are due to small differences (<0.05 K) in starting temperature. As can be seen in the figure, a dramatic decrease in the decay rate is accomplished by this relatively small (0.5 K) change in temperature. A quench at $J = 1.05 \times 10^6$ A/cm^2 results in a 40-fold decrease in the decay rate, while a quench at $J = 0.98 \times 10^6$ A/cm^2 causes the decay rate to fall below our instrumental stability.

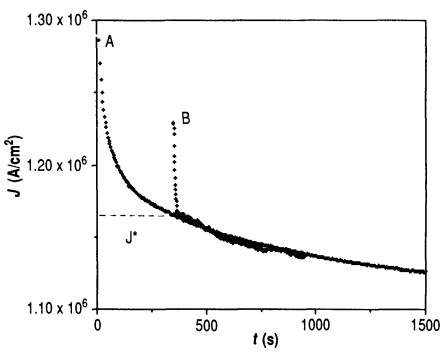

Fig. 5. The relaxation behavior with two different initial conditions at $t_1 \approx 350$ s. Curve A: isothermally relaxed down to $J \approx 1.17 \times 10^6$ A/cm^2 at $t_1 = 420$ s; curve B: quenched from 78 K down to 77.5 K to have the same initial J as for curve A at $t_1 = 420$ s. The time dependence after t_1 of the two curves is identical, indicating that the initial condition at t_1 determines the relaxation behavior thereafter, in confirmation of Eq. 10.

The decay occurring right after quenching down to 77.5 K is well described by the solution, Eq. 10. Shown in Fig. 5 are two relaxation curves. Curve A is the isothermal decay at 77.5 K while curve B is quenched from 78 K to 77.5 K at the current density J^*. It can easily be seen that the relaxation of curve B thereafter follows that of curve A

with a shifted time origin that accounts for the initial condition J^*, just as predicted by Eq. 10. Extrapolating this model, it is expected that the rate of current decay present in the sample after the quench at 80 s shown in Fig. 4 is 1.0 ppm/s. This level of stability would be obtained without a quench only after 20,000 s at 77.5 K, according to Eq. 7.

Therefore, we conclude that the relaxation of magnetic shielding current can be greatly reduced and effectively eliminated if the superconductor is operated at current levels slightly below the critical current density. Since the reduction of the relaxation depends on the operating current reduction level η with a very large power exponent n, such improvements can be made without great sacrifice of the utility of the critical current density. Thus, the relaxation of the magnetic shielding current in the YBCO material is not a serious problem for persistent current applications. A convenient way of achieving this condition, as we have demonstrated, is to simply reduce the operating temperature slightly after the sample enters its critical state.

REFERENCES AND NOTES

1. K. A. Müller, M. Takashige, J. G. Bednorz, *Phys. Rev. Lett.* **58**, 1143 (1987).
2. A. C. Mota, A. Pollini, P. Visani, K. A. Müller, J. G. Bednorz, *Phys. Rev. B* **36**, 401 (1987).
3. I. Morgenstern, K. A. Müller, J. G. Bednorz, *Z. Phys. B* **59**, 33 (1987).
4. Y. Yeshrun and A. P. Malozemoff, *Phys. Rev. Lett.* **60**, 2202 (1988).
5. M. E. McHenry, M. P. Maley, E. L. Venturini, D. L. Ginley, *Phys. Rev. B* **39**, 4784 (1989).
6. C. Rossel, Y. Maeno, I. Morgenstern, *Phys. Rev. Lett.* **62**, 681 (1989).
7. C. W. Hagen, E. Salomons, R. Griessen, B. Dam, *ibid.*, p. 2857.
8. M. J. Ferrari *et al.*, *IEEE Trans. Magn.* **25**, 806 (1989).
9. C. B. Eom *et al.*, *Appl. Phys. Lett.* **55**, 595 (1989).
10. C. P. Bean, *Phys. Rev. Lett.* **8**, 250 (1962).
11. B. Oh *et al.*, *Appl. Phys. Lett.* **51**, 852 (1987).
12. Description of the decay (especially that near T_c at 77 K) is complicated by the fact that the relaxation over many decades of seconds deviates somewhat from the strict logarithmic behavior. This may be a result of the deviation from the critical state current distribution due to the relatively fast decay rate in these materials. The treatment of such a decay process is generally very complicated. For our purposes it is sufficient to ignore such small nonlinearity of M versus $\ln(t)$.
13. J. Z. Sun, C. B. Eom, B. Lairson, J. Bravman, T. H. Geballe, in preparation.

14. The authors thank M. R. Beasley and A. Kapitulnik for in-depth discussions. This work is supported by Electric Power Research Institute under grant RP7911-9, by the Air Force Office of Scientific Research under contract F49620-88-C-004, and by the Stanford Center for Materials Research under NSF-MRL program.

10 November 1989; accepted 22 December 1989

Sedimentary 24-*n*-Propylcholestanes, Molecular Fossils Diagnostic of Marine Algae

J. MICHAEL MOLDOWAN, FREDERICK J. FAGO, CATHY Y. LEE, STEPHEN R. JACOBSON, DAVID S. WATT, NACER-EDDINE SLOUGUI, ALWARSAMY JEGANATHAN, DONALD C. YOUNG

Certain C_{30}-steranes have been used for identifying sedimentary rocks and crude oils derived from organic matter deposited in marine environments. Analysis of a C_{30}-sterane from Prudhoe Bay oil indicates that these C_{30}-steranes are 24-*n*-propylcholestanes that apparently are derived from precursor sterols 24-*n*-propylidene-cholesterols and 24-*n*-propylcholesterol. These widely occurring sterols are biochemically synthesized in modern oceans by members of an order (Sarcinochrysidales) of chrysophyte algae. These data thus imply that C_{30}-sterane biomarkers in sedimentary rocks and crude oils have a marine origin. Screening of a few organic-rich sedimentary rocks and oils from throughout the Phanerozoic suggests that these C_{30}-steranes first appeared and, therefore, their source algae evolved between Early Ordovician and Devonian.

A SERIES OF C_{30}-STERANE EPIMERS containing 11 C atoms in the side chain has been empirically established as a widespread fossil marker for marine organic input to sedimentary rock and petroleum (*1–3*). This concept has been challenged recently (*4*), and some possible C_{30}-sterane precursors have been tentatively identified in lacustrine sediments (*5, 6*). In order to evaluate the origins of these steranes and identify them, we have studied a C_{30}-sterane sourced from marine shale present in a Prudhoe Bay petroleum (*2*).

J. M. Moldowan, F. J. Fago, C. Y. Lee, Chevron Oil Field Research Company, Post Office Box 1627, Richmond, CA 94802.
S. R. Jacobson, Chevron Oil Field Research Company, Post Office Box 446, La Habra, CA 90633.
D. S. Watt, N.-E. Slougui, A. Jeganathan, Department of Chemistry, University of Kentucky, Lexington, KY 40506.
D. C. Young, Chevron Research Company, 576 Standard Avenue, Richmond, CA 94802.

This C_{30}-sterane (12 ppm in the Prudhoe Bay oil) was isolated by a lengthy procedure. The oil was fractionally distilled under vacuum on a spinning band column to provide a narrow-boiling fraction containing the C_{30}-steranes. The fraction was separated by preparative silica gel chromatography, and the saturate fraction was deparaffinated with 5A molecular sieves. Key steps were the removal of certain terpanes (that is, hopanes) with 13X molecular sieves (*7*) and the removal of sterane epimers by chromatography on alumina (*8*). These two steps removed the bulk of the polycyclic biomarkers with physical properties similar to those of the target sterane. Repeated, nonaqueous reversed-phase, high-performance liquid chromatography (HPLC) provided 0.6 mg of 65% pure material. This sample was suitable for comparisons by nuclear magnetic resonance (NMR) with the synthetic materials because all contaminating components were minor constituents, each composing less than 5% of this mixture.

As the standards, we prepared the 5β and 5α epimers of 24-*n*-propylcholestane (structures **1bA** and **1aA** in Fig. 1) and 24-isopropylcholestane (structures **1bD** and **1aD**) by partial synthesis (Fig. 2) as described (*9–12*). Comparisons of the synthetic standards with the isolated C_{30}-sterane by gas chromatography–mass spectrometry (GCMS), ^{13}C NMR, and H NMR indicated that it is (24*R* + 24*S*)-24-*n*-propylcholestane (**1aA**). Its mass spectrum (Fig. 3) is identical to that of synthetic **1aA** and shows the expected D-ring cleavage having a mass-to-charge ratio (m/z) 217 and B-ring cleavage (m/z 304) ions characteristic of a sterane with a $C_{11}H_{23}$ side chain. The ^{13}C NMR spectrum of the isolated material was of sufficient strength to show that it is identical with **1aA**. Both contained a peak at 14.6 ppm diagnostic for the presence of the *n*-propyl group [predicted 14.4 ppm on the basis of Lindeman-Adams parameters (*13*)]. Finally, a fingerprint comparison of 300-MHz H NMR spectra in the methyl resonance region confirmed the structure assignment (Fig. 4).

Steranes are typically found in thermally mature sediments and petroleums as mixtures of stereoisomers at the C-5, 14, 17, 20, and 24 positions (*12, 14*). In order to confirm that the C_{30}-steranes (Fig. 5A) belong to the 24-*n*-propylcholestane series, we prepared an isomerizate by treatment of 24-*n*-propyl-5β-cholestane (**1bA**) with Pd/C at 260°C for 68 hours (*15*). This procedure produced a petroleum-like distribution of sterane epimers (Fig. 5C) nearly identical to and coeluting with the peaks in the m/z = 414 to 217